NASA Contractor Report 198356
AIAA–95–1797

The Decay of Longitudinal Vortices Shed From Airfoil Vortex Generators

Bruce J. Wendt
Modern Technologies Corporation
Middleburg Heights, Ohio

Bruce A. Reichert
Kansas State University
Manhattan, Kansas

Jeffry D. Foster
Iowa State University
Ames, Iowa

June 1995

Prepared for
Lewis Research Center
Under Contract NAS3–27377

National Aeronautics and
Space Administration

THE DECAY OF LONGITUDINAL VORTICES SHED FROM AIRFOIL VORTEX GENERATORS

Bruce J. Wendt*
Modern Technologies Corporation, Middleburg Heights, Ohio, 44130
Bruce A. Reichert†
Kansas State University, Manhattan, Kansas
Jeffry D. Foster‡
Iowa State University, Ames, Iowa

Abstract

An experimental study is conducted to examine the crossplane structure and streamwise decay of vortices shed from airfoil-type vortex generators. The vortex generators are set in a counter-rotating array spanning the full circumference of a straight pipe. The span of the vortex generators above the duct surface, h, is approximately equal to the local turbulent boundary layer thickness, δ. Measurement of three-component mean flow velocity in downstream crossplanes are used to characterize the structure of the shed vortices. Measurements in adjacent crossplanes (closely spaced along the streamwise coordinate) characterize the interaction and decay of the embedded vortices. A model constructed by the superposition of Oseen vortices is compared to the data for one test case.

Motivation and Research Objectives

Modern design characteristics of aircraft engine inlets, diffusers, and associated ducting components include large amounts of streamwise curvature coupled with rapid axial variations in cross-sectional area. The flow performance of these components is degraded by the development of strong internal secondary flows and boundary layer separations. Surface mounted vortex generators are an effective means of alleviating these problems. Recent experimental work at NASA Lewis has explored the strategy of using vortex generator induced flows to counter deleterious secondary flow development and boundary layer separation inside a diffusing S-duct.[1] Dramatic improvements in total pressure recovery and exit plane flow distortion were demonstrated. An experimental program to test candidate designs for the new High Speed Research (HSR) diffuser is currently in the planning stages. Surface mounted vortex generators are being considered as a means of enhancing the performance of the HSR diffuser.

Arrays of vortex generators may be studied to determine what vortex generator size, spacing, and streamwise location produces optimal flow conditions in a particular duct operating at a particular condition. This can be done experimentally, as in Reference 1. However, due to the large number of possible vortex generator array parameter variations, optimization may be best suited for computational work. The effort required for a computational study hinges on the manner in which the vortex generators are represented in the analysis. A particularly effective approach is to model the shed vortex immediately downstream of the vortex generator, rather than model the vortex generator by including it in the gridwork of the duct. The advantage here lies in the fact that a newly formed vortex may be accurately represented as a streamwise vorticity or crossplane velocity distribution having a simple exponential form. This is the approach taken in recent work by Anderson and Gibb,[2] and Anderson and Farokhi,[3] where multiple vortex generator array geometries in a diffusing S-duct inlet were examined using a parabolized Navier-Stokes (PNS) solver. The crossplane structure of embedded vortices shed from vortex generators may be characterized in terms of quantities known as vortex "descriptors". The modelled vortices are based on these descriptors. Following the work of Westphal *et al.*[4] we identify three descriptors:

1. Peak streamwise vorticity: ω_{max} is an indication of vortex concentration. The larger the magnitude of peak vorticity, the thinner and more concentrated the vortex structure.
2. The crossplane location of ω_{max}. This location corresponds to the center of the vortex, the point about which the vortex spins.
3. Circulation: Γ is a measure of the vortex strength.

In an ongoing research program at NASA Lewis, a set of experimental studies are being conducted to acquire the database necessary for simple analytical modelling of all types of common vortex generators. A recently completed study on the sub-boundary layer scaled "wishbone" vortex generator has provided detailed datasets and corresponding descriptors for the modelling of this type of vortex generator over a limited Mach number and Reynolds number range.[5] This paper describes a similar experimental study of blade or airfoil-type vortex generators. The

*Resident Research Engineer at NASA Lewis, Cleveland Office, 7530 Lucerne Drive, Islander Two, Suite 100, Member AIAA.

†Associate Professor, Department of Mechanical Engineering, Member AIAA.

‡NASA Resident Research Associate at Lewis Research Center and Graduate Student, Mechanical Engineering Department at Iowa State University.

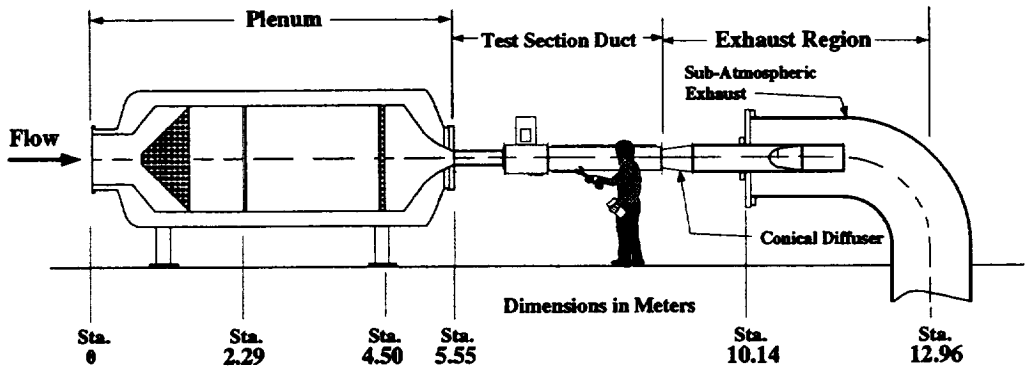

Figure 1 The Internal Fluid Mechanics Facility of NASA Lewis.

vortex generators are mounted in a symmetric counter-rotating array which spans the full interior circumference of a circular pipe. A thin turbulent boundary layer is developed upstream of this array. The boundary layer thickness, δ, is approximately 4% of the pipe diameter, d, at the axial location of the vortex generators.

The primary objective of this study is to examine the crossplane structure and streamwise decay of vortices shed from airfoil-type vortex generators. Vortex descriptors are derived from crossplane measurements of three-component mean flow velocities acquired with a rake probe. Crossplane grid resolution is greater than in previous studies, and axial separation (Δz) between adjacent crossplanes is much finer, with $\Delta z \approx \delta$. Simple analytical models of the induced crossplane distributions of velocity and vorticity are constructed with the vortex descriptors. These will be compared against the data.

Facilities and Procedures

Test Facility

This study is conducted in the Internal Fluid Mechanics Facility (IFMF) of NASA Lewis. The IFMF is a subsonic facility designed to investigate a variety of duct flow phenomena. The facility, as it is configured for this test, is illustrated in Figure 1. Air is supplied from the surrounding test cell to a large settling chamber containing honeycomb and screens. At the downstream end of the settling chamber the airstream is accelerated through a contraction section (having a cross-sectional area reduction of 59 to 1) to the test section duct. The test section duct consists of a straight circular pipe of inside diameter $d = 20.4$ cms. After exiting the test section duct the airstream enters a short conical diffuser and is then routed to a discharge plenum which is continuously evacuated by central exhauster facilities. The Mach number range in the test section duct is between 0.2 and 0.8 with corresponding Reynolds numbers (based on pipe diameter) between 0.95 and 3.80 million. Mass flows are between 3 and 7 kgs/sec. More information on the design and operation of the IFMF may be found in the report of Porro *et al.*[6]

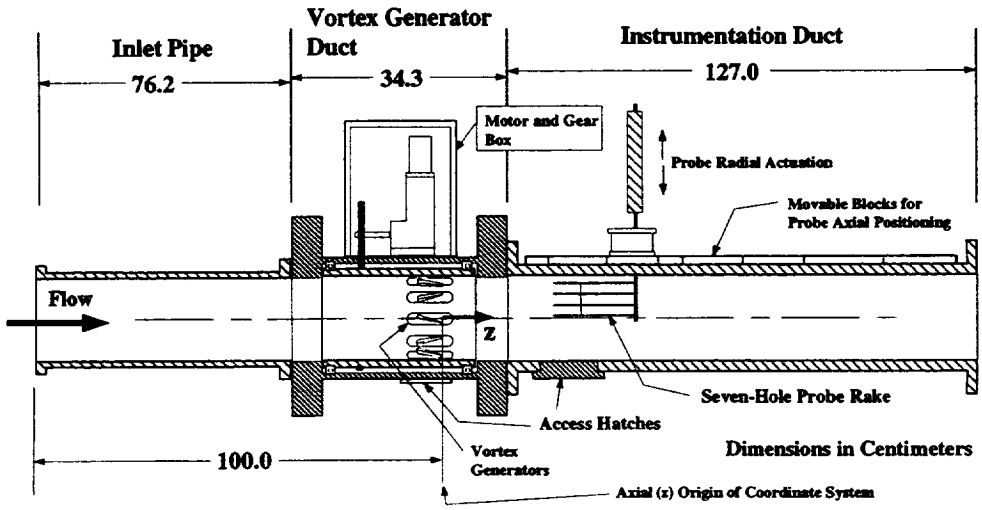

Figure 2 A cut-away sketch of the test section duct.

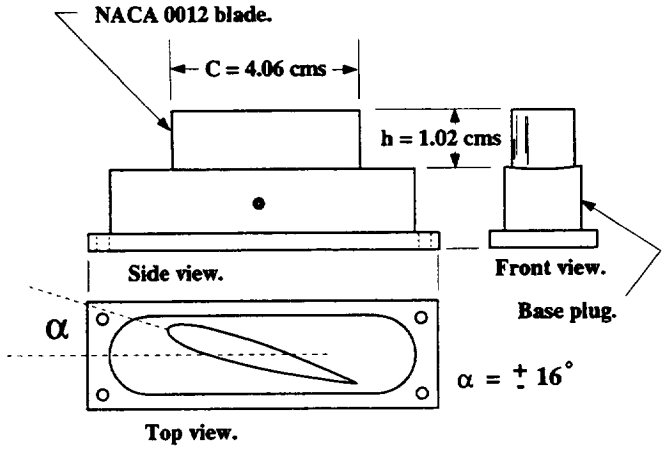

Figure 3 The airfoil vortex generator.

Research Instrumentation and Test Parameters

Figure 2 is a detailed sketch of the various test section components.

A short section of straight pipe (labeled "inlet pipe" in Figure 2) connects the exit of the facility contraction to the duct segment containing the vortex generator array. Static pressure taps located on the surface of the inlet pipe allow the nominal core Mach number in the test section to be set and monitored.

The duct portion with vortex generators is referred to as the "vortex generator duct". The inside surface of the vortex generator duct (and hence the attached vortex generator array) rotates about an axis coinciding with the test section centerline. A rotation of 360 degrees is possible. The rotation is driven by a motor and gear located in an airtight box above the vortex generator duct.

A vortex generator is illustrated in Figure 3. These vortex generators consist of an airfoil-shaped blade (with a NACA 0012 profile) mounted perpendicular to the surface of a base plug. The surface of the base plug is contoured to the inside radius of the vortex generator duct. Both blade and plug are machined from an aluminum alloy using a wire cutting (electric discharge machining) process.

The vortex generator array consists of 12 blades, identical in geometry, but alternating in angle of attack, $\alpha = \pm 16$ degrees. Figure 4 is a downstream view of the vortex generator duct showing the array of vortex generators. The vortex generators are equally spaced, circumferentially, at *mid-chord*. $\Delta\theta_b$ between the mid-chord position of adjacent blades is 30 degrees, where θ is the circumferential coordinate.

The coordinate system used in this study originates in the vortex generator duct. $z = 0$ coincides with the trailing edge of the vortex generator array. The axial locations of downstream (r, θ) crossplanes are given in terms of blade chord, c. For example, the first survey location possible is the (r, θ) crossplane located at $z = 0.38c$, where $c = 4.06$ cms.

The duct segment downstream of the vortex generator duct is stationary (non-rotating). This test section segment is referred to as the "instrumentation duct". The flowfield measurements are acquired in this duct through the use of a radially actuated rake-probe indicated in Figure 2. To acquire data in an (r, θ) crossplane, the rake-probe is actuated over a radial segment extending from the duct wall to the duct centerline. The vortex generator duct and vortex generator array are then rotated an increment in circumferential position, $\Delta\theta$, and the radial survey repeated. In this manner pie-shaped pieces of the flowfield are examined. A narrow slot running the approximate length of the instrumentation duct allows the rake-probe to be located at various downstream crossplanes. A series of slot-sealing blocks determines the allowable axial location of survey crossplanes, z_i:

$$z_i = 0.38c, 1.00c, ..., 10.38c, \\ 14.75c, 15.38c, ..., 24.75c. \quad (1)$$

The rake-probe consists of 4 seven-hole probe tips spaced 2.54 cms apart. These probes are calibrated in accordance with the procedure outlined by Zilliac.[7] The flow angle range covered in calibration is $\pm 60°$ in both pitch and yaw for the probe tip closest to the wall. The calibration range for the outer 3 tips is approximately $\pm 30°$. Uncertainty in flow angle measurement is $\pm 0.7°$ in either pitch or yaw, for flow angle magnitude below 30 degrees (pitch and yaw flow angle magnitude did not exceed 30 degrees in this study). The corresponding uncertainty in velocity magnitude is approximately $\pm 1\%$ of the core velocity, v_{zc}.

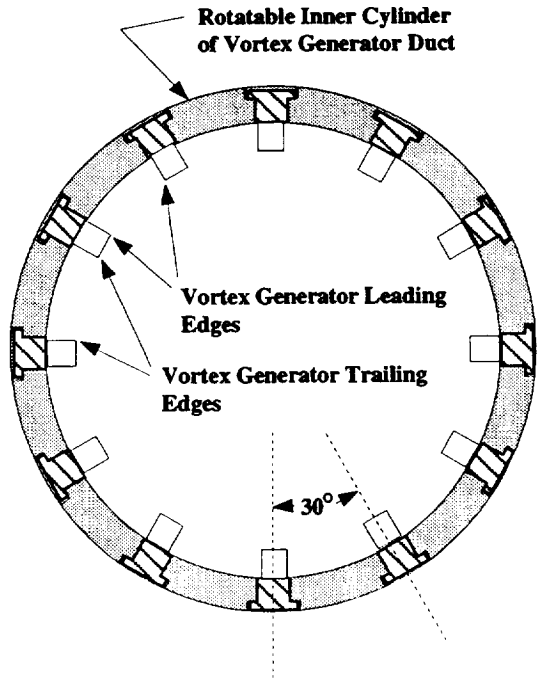

Fig. 4 The vortex generator array.

Experimental Results

Figures 5a-k illustrate the experimental results. On the left in Figure 5 are vector plots of crossplane (or "transverse") velocity. The radial axis represents distance from the wall, in centimeters, and the circumferential axis represents angular position in degrees. In the middle of Figure 5 are the corresponding contours of primary velocity ratio, v_z/v_{zc}, where $v_{zc} \approx 85$ m/sec is the core velocity of the pipe (this corresponds to a nominal test section Mach number $M = 0.25$). On the right hand side of Figure 5 are plots of streamwise vorticity. These results are derived from the transverse velocity data following the relation:

$$\omega_z = \frac{\delta v_\theta}{\delta r} + \frac{v_\theta}{r} - \frac{1}{r}\frac{\delta v_r}{\delta \theta}, \qquad (2)$$

where ω_z is the streamwise component of vorticity, and (v_r, v_θ) are the transverse components of velocity in the radial and circumferential coordinates, respectively. Finite difference formulas are used to represent the spatial derivatives in Eq. (2). Solid contour lines represent negative vorticity, dashed lines are positive. The axial location of each crossplane is indicated in Figure 5.

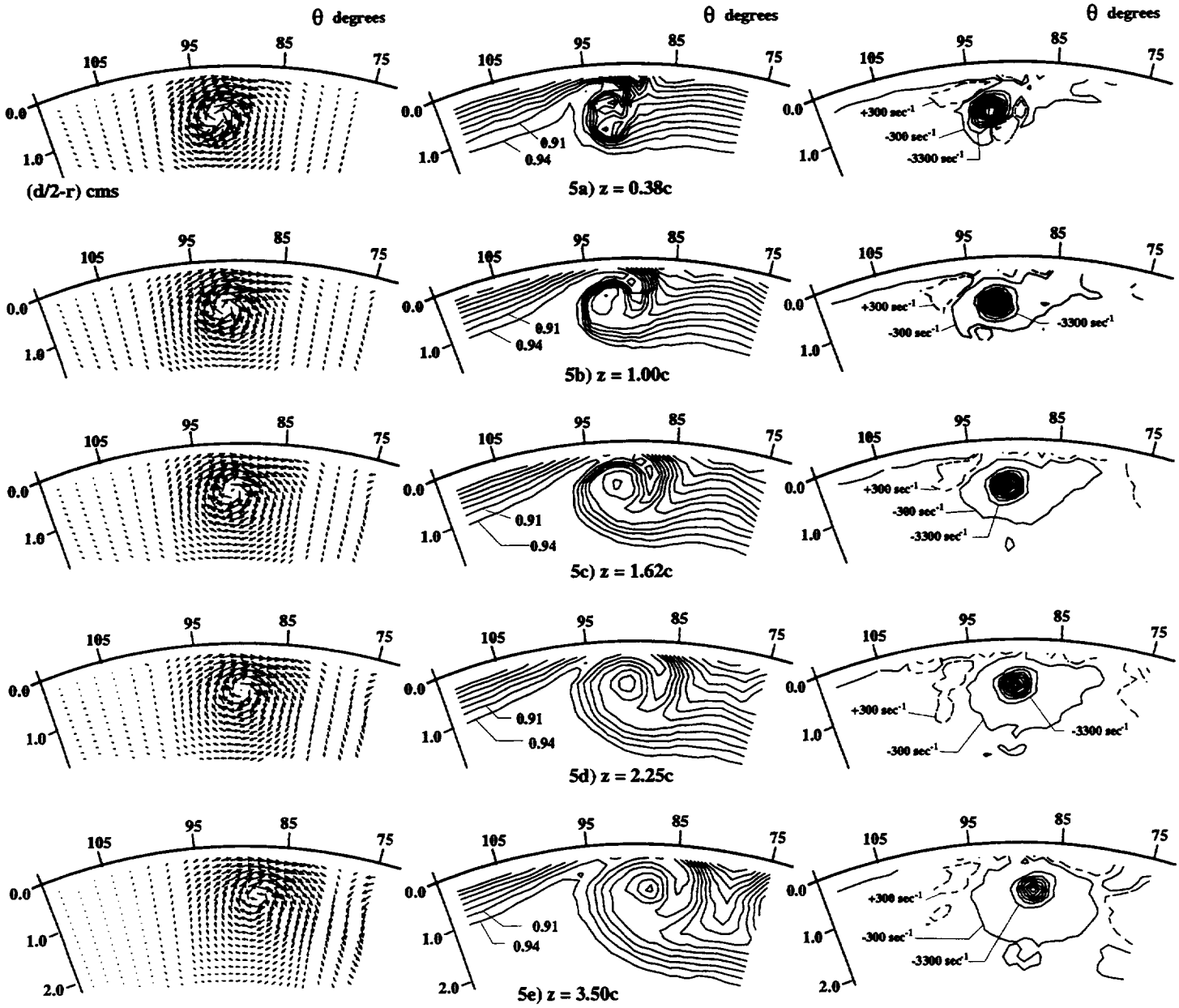

Figure 5 Velocity and streamwise vorticity results. (Continued . . .)

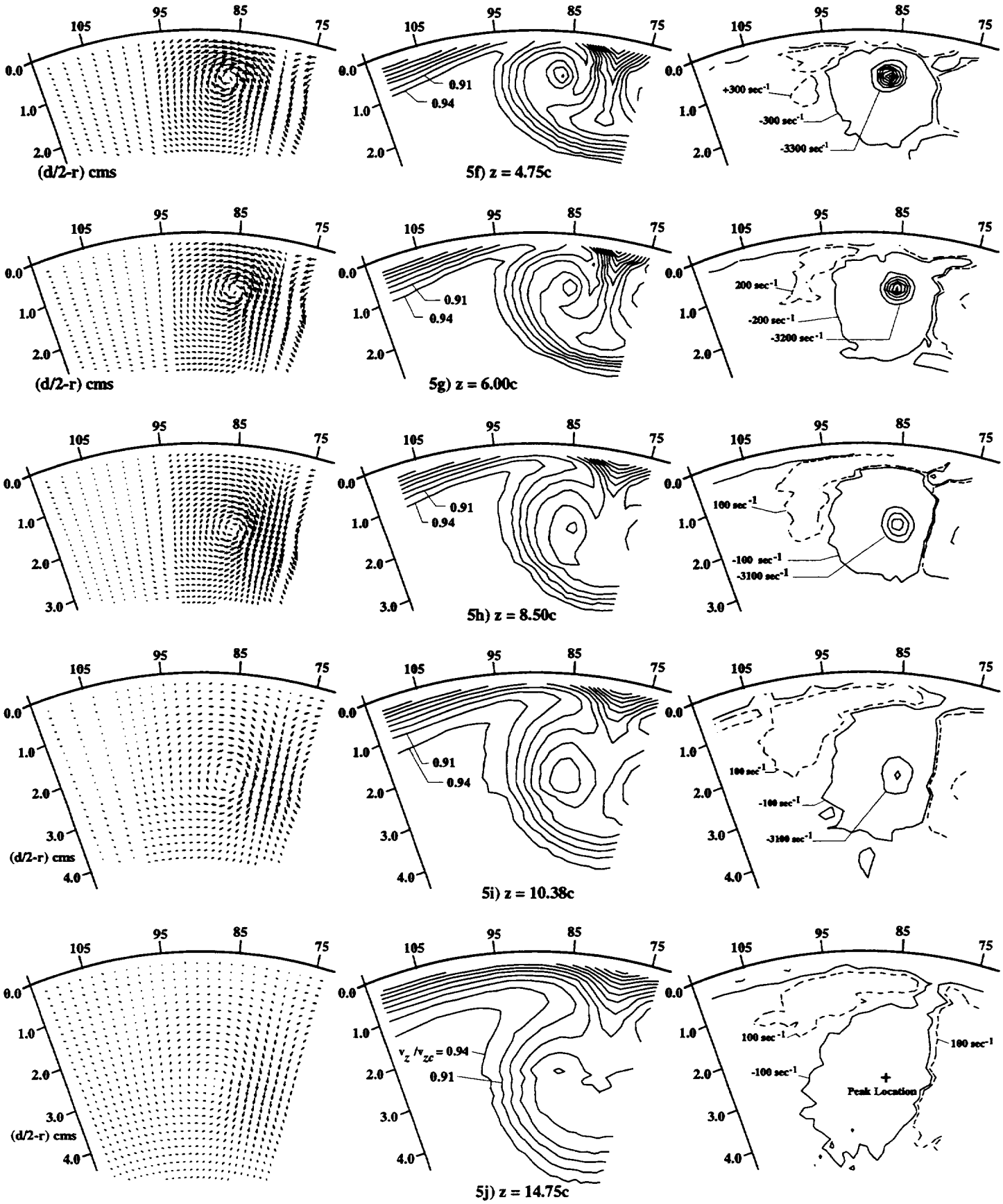

Figure 5 Velocity and streamwise vorticity results. (Continued . . .)

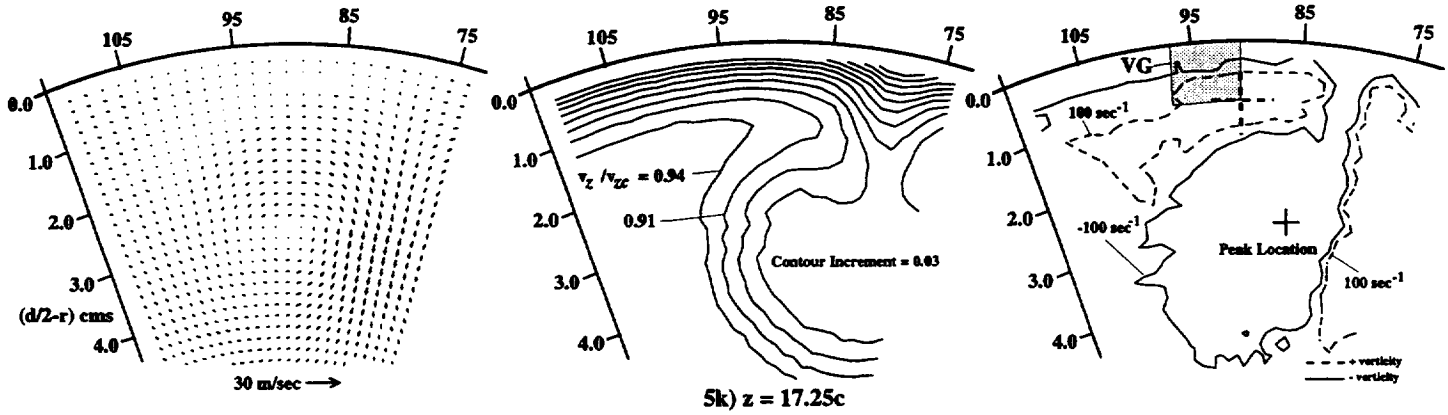

Figure 5 Velocity and streamwise vorticity results.

Crossplane grid resolution for these surveys is based on the size of the vortex core. At axial locations just downstream of the vortex generator the vortex core is small and highly concentrated with large secondary velocities present. To properly capture vortex structure the grid resolution must be greater here than at locations far downstream where the developing core has grown larger and more diffuse. Thus, in Figures 5a-h, $\Delta r = 1.3$ mm and $\Delta\theta = 1.0$ degree in the vicinity of the core; and in Figures 5i-k, $\Delta r = 1.7$ mm and $\Delta\theta = 1.5$ degrees. Although the full pie-sector (from pipe wall to centerline) was surveyed, only the portion of the grid closest to the wall and embedded vortex is plotted. This is done to save space in Figure 5. The survey grid covers somewhat more than a 30 degree sector of the pipe cross-section. A 30 degree sector coincides with the circumferential domain occupied by one vortex generator (hence the single vortex observed in each of the crossplane plots of Figure 5). For the counter-rotating arrangement of vortex generators tested in this study the full flowfield is (ideally) a 12 unit multiple of this pie-sector, alternating in the rotation of the shed vortex from one 30 degree sector to the next. The circumferential component of velocity (v_θ), and hence the crossflow, is expected to vanish at the boundaries of the pie-sector where the influence of the neighboring vortex begins. We note from Figure 5 (particularly Figures 5e-k) this is approximately the case, with the boundary between the domain of the illustrated vortex and the domain of its nearest neighbor located at $\theta = 79$ or 80°. A portion of the adjacent sector ($\theta \leq 80°$) and neighboring vortex is visible in Figure 5. The illustrated vortex and its neighbor constitute an *upflow* pair of counter-rotating vortices. Upflow pairs have a strong tendency to pull together and lift away from the wall, and this is clearly evident in Figure 5.

In Figures 5a-b we see a strong, concentrated vortex structure. At the $z = 1.00c$ position (Figure 5b) contours of primary velocity ratio show two distinct regions of v_z deficit in the vicinity of the vortex core. One region appears to be a convection of low momentum boundary layer fluid found near the wall and wrapping around the core on the right-hand side; the other region is associated with the central portion of the vortex core. This characteristic double deficit persists downstream of the $z = 1.00c$ position. Interestingly, however, the central core v_z deficit is not nearly as pronounced further upstream at the $z = 0.38c$ position. Here the central or core primary velocity structure is much more complex, with what appears to be two separate deficit regions. The primary velocity ratio contours in Figure 5 also illustrate the alternate thinning and thickening of the boundary layer in the core downwash and upwash, respectively. The upwelling of boundary layer fluid produced by the strong convection of the counter-rotating vortex pair is quite pronounced at the downstream survey locations. In Figure 5k an indication of the crossplane profile of the vortex generator is provided. The cruciform of dashed lines identifies the trailing edge tip.

The three previously defined structural descriptors of the embedded vortex originate from the streamwise vorticity and transverse velocity data in the crossplane. ω_{max} is located at some grid point having coordinates (r_{max}, θ_{max}). The vortex circulation Γ is calculated by first isolating the region of core vorticity in the data field. This is done by referring to the contour plots of vorticity in Figure 5. A path enclosing the region of core vorticity is defined. The outer boundary of the core is taken to be the location where streamwise vorticity is 1% of the peak core value. The circulation is then calculated according to:

$$\int_{path} \mathbf{V} \cdot \mathrm{ds}, \qquad (3)$$

where $\mathbf{V}$ is the velocity vector in the crossplane, and s refers to the path coordinate. By using closed paths composed of line segments in the r or θ coordinate directions the circulation is easily determined.

Axial Location, z/c	Circulation m^2/sec	Peak Vorticity sec^{-1}	Crossplane Location of Peak Vorticity (cms, deg)*	Kinetic Energy Ratio
Inviscid Airfoil Theory Est.	-0.753	—	(1.02, 90.5)**	—
0.38	-0.733	-34655	(0.89, 93)	0.0078
1.00	-0.722	-35714	(0.89, 92)	0.0072
1.62	-0.698	-33896	(0.89, 91)	0.0067
2.25	-0.688	-30488	(0.89, 90)	0.0064
3.50	-0.671	-24258	(0.89, 88)	0.0057
4.75	-0.663	-22807	(1.02, 86)	0.0050
6.00	-0.646	-19179	(1.27, 85)	0.0045
8.50	-0.596	-10679	(1.78, 84)	0.0034
10.38	-0.543	-6606	(2.29, 84)	0.0028
14.75	-0.408	-2748	(2.79, 86)	0.0014
17.25	-0.360	-1766	(2.79, 86)	0.0010
Uncertainty	± 0.007	± 225	± (0.04,0.3)	± 0.0003

* This column lists (d/2-r, theta) where d = 20.4 cms = pipe diameter. ** Trailing edge tip of vortex generator.

Table 1 - The decay of the symmetric array.

In addition to the vortex descriptors, an integral parameter known as the "kinetic energy ratio" (μ) is also calculated for each crossplane data grid. μ is defined as follows:

$$\mu = KE_t/KE_s,$$
$$KE_t = \frac{1}{A_p}\int\int \rho(v_r^2 + v_\theta^2)\, dA, \qquad (4)$$
$$KE_s = \frac{1}{A_p}\int\int \rho v_z^2\, dA,$$

where ρ is the fluid density, and A_p is the area of a 30 degree pie-sector in the pipe. Table 1 lists the three descriptors, and kinetic energy ratio for the vortex captured in the 11 crossplane grids shown in Figure 5. The units of Table 1 are SI. The "inviscid airfoil theory" estimate of vortex circulation is derived from Prandtl's[8] result for a wing of elliptical planform:

$$\Gamma = \frac{\pi c v_{zc} \alpha}{1 + 2/AR}, \qquad (5)$$

where the aspect ratio of the vortex generator is $AR = 4 \times span/\pi c$. Note that when performing this calculation, use $span = 2h$ (refer to Figure 3), due to the wall effect or "image vortex generator". Uncertainty estimates for all listed quantities are given in Table 1. These are derived by combining the uncertainties in measured velocities and probe placement in accordance with the procedure outlined by Moffat.[9]

The results listed in Table 1 are plotted in Figures 6 a-c.

Figure 6a plots the axial distribution of embedded vortex circulation. The shape of the curve demonstrates two mechanisms of circulation decay affecting the embedded vortex. This is similar to what is outlined in an earlier study on the decay behavior of embedded vortex arrays on a flat plate.[10] Just downstream of the vortex generator, the viscous vortex core is close to the wall and isolated (by surrounding regions of near-zero streamwise vorticity) from neighboring vorticies. Refer to Figures 5a-d. The dominant mechanism of circulation decay is through the action of wall friction, which sets up a spanwise component of wall shear stress opposing the rotation of the core. As the neighbor vortex core draws near and lifts the vortex away from the wall, the rate of circulation decay due to wall friction effects drops (Figures 5e-f). When the core vorticity profiles of vortex and neighbor begin to "touch" (recall that they are of opposite sign) another mechanism of circulation decay begins to dominate (Figures 5g-k). This is circulation loss through *vorticity diffusion across core boundaries*. Rapid losses in circulation, peak vorticity, and kinetic energy ratio occur downstream of the location where this mechanism of circulation decay is prominent.

Figures 6b-c plot the decay of peak vorticity and kinetic energy ratio as given in Table 1.

Modelling Results

The large number of parameters to consider when designing a vortex generator array for an aircraft component, such as a wing or inlet, has the implication that experimental work on optimum array geometries is often slow and expensive. This fact has motivated a few workers in computational fluid mechanics to assist in the optimizing problem by including a means of representing vortex generators in their codes. A simple and effective means of doing this is to employ a model for the crossplane velocity or vorticity field induced by the generators. This is the approach taken in recent work by Anderson *et al.*[3, 2] who examined multiple vortex generator array geometries in a diffusing S-duct inlet using a parabolized Navier-Stokes (RNS) solver. A similar inclusion of embedded vortices in a full Navier-Stokes (FNS) code was

implemented by Cho and Greber[11] for a constant area circular duct and a diffusing S-duct geometry. The advantage of this approach lies in the fact that a newly formed vortex may be accurately represented in this manner.

Experimental workers concerned with embedded vortices have often noticed the close similarity of observed crossplane vortex structure to simple two-dimensional models of vortices. Inviscid or "potential" models were first applied to results obtained in subsonic diffusers by Grose and Taylor.[12] Later, Pearcy[13] would develop embedded vortex interaction models based on the inviscid representation of embedded vortex structure. Eibeck and Eaton[14] compared the structure of a single embedded vortex to that of the patchwork "Rankine" model vortex. Studies by Pauley and Eaton[15] and Wendt *et al.*[10, 16] have made comparisons to the "ideal viscous" or "Oseen" model.

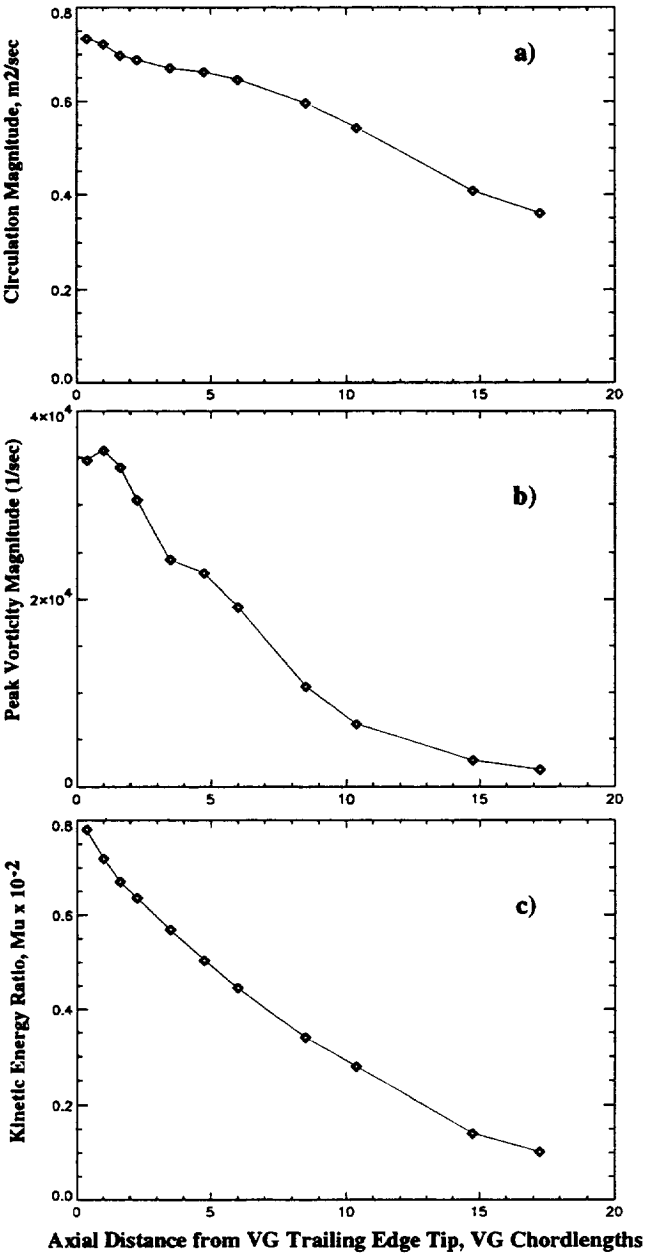

Figure 6 Decay Behavior of the Symmetric Array.

Let us now examine the equations of the Oseen vortex and show how the array of embedded vortices examined in this study may be represented using a simply constructed model based on this vortex.

The Oseen Model of the Embedded Vortex Array

The two-dimensional Oseen model of a viscous vortex represents the time dependent decay of a potential vortex where the velocity at the origin ($r = 0$) is forced to zero at time $t = 0$. A single isolated vortex centered on the crossplane origin has velocity components (in cylindrical coordinates):

$$v_r = 0, \qquad v_\theta = \frac{\Gamma}{2\pi r}\left(1 - e^{r^2/(4\nu t)}\right), \tag{6}$$

where Γ is the vortex circulation and ν the laminar coefficient of kinematic viscosity. Following Squire[17] the unsteady solution is transformed to a steady one by relating the decay time to the distance between the vortex generator tip and the crossplane of interest ($z - z_0$):

$$t \approx \frac{z - z_0}{U_\infty}. \tag{7}$$

For an isolated turbulent vortex i located at:

$$(x_i, y_i = r_i \cos\theta_i, r_i \sin\theta_i) \tag{8}$$

the velocity components in the crossplane can be written in terms of the vortex descriptors.[18] In cartesian coordinates:

$$v_i = \frac{\Gamma_i (x - x_i)}{2\pi R_i^2} F_i, \qquad w_i = -\frac{\Gamma_i (y - y_i)}{2\pi R_i^2} F_i, \tag{9}$$

where:

$$R_i^2 = (x - x_i)^2 + (y - y_i)^2, \tag{10}$$

and:

$$F_i = 1 - \exp\left\{-\frac{\pi \omega_i^{max}}{\Gamma_i} R_i^2\right\}. \tag{11}$$

The vorticity field is given by:

$$\omega_i^z = \omega_i^{max}(1 - F_i). \tag{12}$$

We can superimpose solutions for a representation of the pipe wall and other array vortices. Figure 7 illustrates this construction. Each of the 12 vortices in the array is located a distance R_v from the pipe centerline. To represent the influence of the wall on each vortex in the array, an image vortex is superimposed a distance $R_{im} = R^2/R_v$ in accordance with the procedure outlined by Milne-Thomson.[19] The angle $\epsilon = 30°$ for all test cases in this study. In each test case, the descriptors of all vortices

and images are determined from symmetry following Table 1 and Figure 7. For example, the angle ζ between the center of the vortex and the line of flowfield symmetry between upflow vortices is repeated at regular intervals around the pipe. Also, the magnitude of circulation and peak vorticity is assumed to be the same for all vortices and images in each test case, differing only in sign, depending on the rotation of the vortex or image vortex. With these constraints on the array geometry the equations of the model are simply:

$$v = \sum_{i=1}^{12} (v_i + v_{i\,im}),$$
$$w = \sum_{i=1}^{12} (w_i + w_{i\,im}), \tag{13}$$

where the $i\,im$ subscript denotes the appropriate expression from Equations 9–11 for the image vortex i.

Data and Model Comparisons

The data and model are compared at the $z = 1.00$ chord survey position. The vortex descriptors are taken directly from Table 1 and used in Equation 13. Figures 8a-b illustrate the resulting comparison. Figure 8a compares the transverse velocity and streamwise vorticity fields of the data (top) and model (bottom) vortex arrays. Note the close similarity of the transverse velocity fields. Since the model is two-dimensional, representation of the secondary (or "wall") generation of opposite-sign vorticity, found in the data, is not possible. This is evident in the comparisons of the streamwise vorticity fields. Define

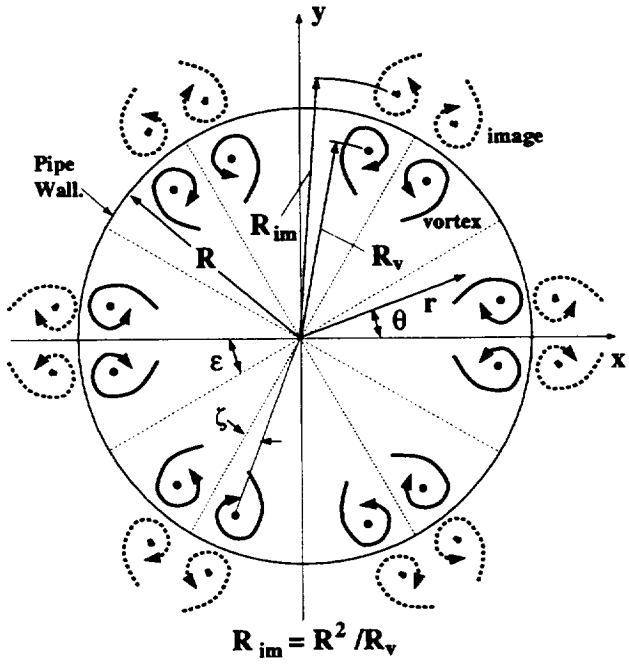

Figure 7 The construction of an Oseen model of an array of 12 symmetrically placed vortices in a pipe.

a fit parameter based on the transverse velocity:

$$fit = \frac{\left\| \vec{V}_{data} - \vec{V}_{model} \right\|}{\left\| \vec{V}_{data} \right\|}. \tag{14}$$

Figure 8b is a contour plot of this parameter over the survey grid. The shaded areas represent regions where the fit parameter exceeds 1.00 (or "100 percent"). Limited probe resolution of the weak velocities in these areas

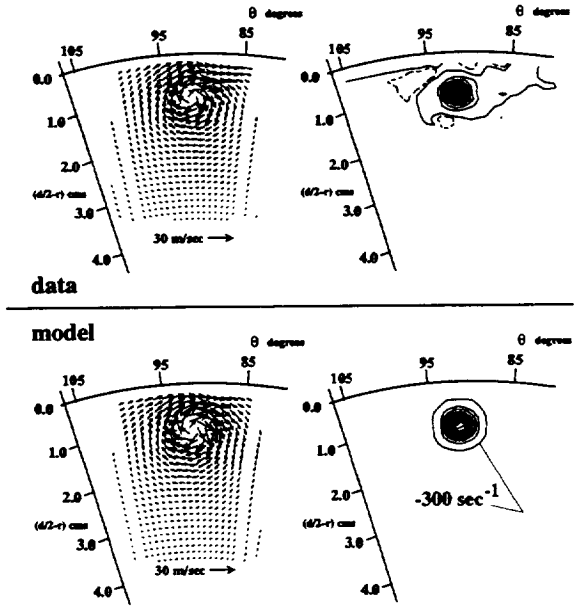

a) Transverse Velocity and Streamwise Vorticity Comparisons

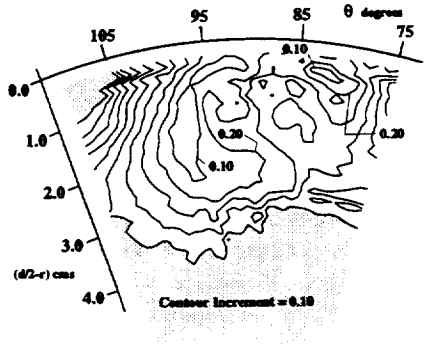

b) Contours of Fit Parameter

Figure 8 A comparison of the data and model. a) data and model transverse velocity and streamwise vorticity fields, b) contours of the fit parameter (Equation 14).

is the most probable cause of the large discrepancies. It is encouraging to note that where the convective effects of the vortex are strongest the model best represents the data. The viscous core, the region of strong crossflow underneath the core, and the upwash and downwash regions to either side, are all within the 40 percent contour of the fit parameter.

Summary

An experimental study is conducted to examine the crossplane flow structure, interaction, and streamwise decay of an array of counter-rotating longitudinal vortices embedded in a turbulent boundary layer on the wall of a straight pipe. The vortices are shed from a symmetric array of NACA 0012 airfoil vortex generators. The span of the vortex generators above the flow surface, h, is approximately equal to the local boundary layer thickness, δ. The ratio of boundary layer thickness to pipe diameter is $\delta/d = 0.04$, and the core Mach number = 0.25. Measurements of mean three-component velocities in downstream crossplanes are used to characterize the structure of the shed vortices. Measurements in adjacent crossplanes, closely spaced along the axial coordinate, characterize the vortex-to-vortex and vortex-to-wall interaction and streamwise decay of vortex structure.

Downstream of the vortex generators, the shed vortices are observed forming upflow pairs. The convective effects of each vortex on its neighbor drive the pair away from the wall, initially mitigating the wall-friction driven decay of circulation and peak vorticity. Further downstream, the rate of decay is enhanced when vorticity diffusion occurs across core boundaries in the closely spaced vortex pairs.

The velocity field of the embedded vortex is well represented with a model constructed by the superposition of Oseen vortices. Variation in the transverse vector field between the data and model is less than 40 percent in crossplane regions containing the vortex core, vortex downwash, upwash, and near-wall crossflows.

Future Work

This study will be extended to examine the dependence of vortex generator geometry (h, c, α) and impinging flow conditions $(Mach, \delta)$ on the shed vortex descriptors. A paper on this topic should be ready early in 1996.

Acknowledgements

This project was supported with funding from NASA Lewis and the National Research Council. The authors would like to acknowledge the mechanical skills of Bill Darby and Bob Ehrbar (NASA's Test Installation Division) and the systems engineering support of Robert Gronski (NYMA). Charles Wasserbauer (also of NYMA) provided engineering and operational support. Design engineering service was provided by Arthur Sprungle of NASA Lewis. Dr. Warren R. Hingst provided valuable insight into the test section design. A special thank you to Bernie Anderson, whose vortex generator computations aided greatly in determining the grid location and resolution for this study, and to Mr. R. Brautigan for his insights.

References

[1] Reichert, B. A. and Wendt, B. J., "Improving Diffusing S-Duct Performance by Secondary Flow Control," AIAA Paper 94-0365, Jan. 1994.

[2] Anderson, B. H. and Gibb, J., "Application of Computational Fluid Dynamics to the Study of Vortex Flow Control for the Management of Inlet Distortion," AIAA Paper 92-3177, July 1992.

[3] Anderson, B. H. and Farokhi, S., "A Study of Three Dimensional Turbulent Boundary Layer Separation and Vortex Flow Control Using the Reduced Navier-Stokes Equations," Turbulent Shear Flow Symposium tech. rep., 1991.

[4] Westphal, R. V., Pauley, W. R., and Eaton, J. K., "Interaction Between a Vortex and a Turbulent Boundary Layer-Part 1: Mean Flow Evolution and Turbulence Properties," NASA TM 88361, Jan. 1987.

[5] Wendt, B. J. and Hingst, W. R., "Measurements and Modeling of Flow Structure in the Wake of a Low Profile Wishbone Vortex Generator," AIAA Paper 94-0620, Jan. 1994.

[6] Porro, A. R., Hingst, W. R., Wasserbauer, C. A., and Andrews, T. B., "The NASA Lewis Research Center Internal Fluid Mechanics Facility," NASA TM 105187, Sept. 1991.

[7] Zilliac, G. G., "Modelling, Calibration, and Error Analysis of Seven-Hole Probes," *Experiments in Fluids*, Vol. 14, 1993, pp. 104–120.

[8] Prandtl, L., "Applications of Modern Hydrodynamics to Aeronautics," NACA Report 116, 1921.

[9] Moffat, R. J., "Contributions to the Theory of Single-Sample Uncertainty Analysis," *Transactions of the ASME*, Vol. 104, June 1982, pp. 250–258.

[10] Wendt, B. J., Greber, I., and Hingst, W. R., "The Structure and Development of Streamwise Vortex Arrays Embedded in a Turbulent Boundary Layer," AIAA Paper 92-0551, Jan. 1992.

[11] Cho, S. Y. and Greber, I., *Three Dimensional Compressible Turbulent Flow Computations for a Diffusing S-Duct With/Without Vortex Generators*, Ph.D. Dissertation, Case Western Reserve University, Cleveland, OH, Nov. 1992.

[12] Grose, R. M. and Taylor, H. D., "Theoretical and Experimental Investigation of Various Types of Vortex Gener-

ators," United Aircraft Corporation Research Department Report R-15362-5, East Hartford, CT, Mar. 1954.

[13]Pearcy, H. H., "Shock-Induced Separation and its Prevention by Design and Boundary Layer Control," *Boundary Layer and Flow Control*, Vol. 2, edited by G. V. Lachmann, Pergamon Press, New York, 1961, pp. 1166–1344.

[14]Eibeck, P. A. and Eaton, J. K., "An Experimental Investigation of the Heat-Transfer Effects of a Longitudinal Vortex Embedded in a Turbulent Boundary Layer," Stanford University Tech. Rep. MD-48, Stanford, CA, Nov. 1985.

[15]Pauley, W. R. and Eaton, J. K., "The Fluid Dynamics and Heat Transfer Effects of Streamwise Vortices Embedded in a Turbulent Boundary Layer," Stanford University Tech. Rep. MD-51, Stanford, CA, Aug. 1988.

[16]Wendt, B. J. and Hingst, W. R., "Flow Structure in the Wake of a Wishbone Vortex Generator," *AIAA Journal*, Vol. 32, Nov. 1994, pp. 2234–2240.

[17]Squire, H. H., "The Growth of a Vortex in Turbulent Flow," *Aeronautical Quarterly*, Vol. 16, Aug. 1965, pp. 302–306.

[18]Wendt, B. J., Greber, I., and Hingst, W. R., "The Structure and Development of Streamwise Vortex Arrays Embedded in a Turbulent Boundary Layer," NASA TM 105211, Sept. 1991.

[19]Milne-Thomson, L. M., *Theoretical Hydrodynamics*, 4th ed., Macmillan, New York, 1960.

REPORT DOCUMENTATION PAGE

Form Approved
OMB No. 0704-0188

1. AGENCY USE ONLY (*Leave blank*)	2. REPORT DATE	3. REPORT TYPE AND DATES COVERED
	June 1995	Final Contractor Report

4. TITLE AND SUBTITLE

The Decay of Longitudinal Vortices Shed From Airfoil Vortex Generators

5. FUNDING NUMBERS

WU-505-62-52
C-NAS3-27377

6. AUTHOR(S)

Bruce J. Wendt, Bruce A. Reichert, and Jeffry D. Foster

7. PERFORMING ORGANIZATION NAME(S) AND ADDRESS(ES)

Modern Technologies Corporation
Cleveland Office
7530 Lucerne Drive
Islander Two, Suite 100
Middleburg Heights, Ohio 44130

8. PERFORMING ORGANIZATION REPORT NUMBER

E-9730

9. SPONSORING/MONITORING AGENCY NAME(S) AND ADDRESS(ES)

National Aeronautics and Space Administration
Lewis Research Center
Cleveland, Ohio 44135-3191

10. SPONSORING/MONITORING AGENCY REPORT NUMBER

NASA CR-198356
AIAA-95-1797

11. SUPPLEMENTARY NOTES

Prepared for the 13th Applied Aerodynamics Conference sponsored by the American Institute of Aeronautics and Astronautics, San Diego, California, June 19–22, 1995. Bruce J. Wendt, Modern Technologies Corporation, 7530 Lucerne Drive, Islander Two, Suite 100, Middleburg Heights, Ohio 44130 (research started while National Research Council—NASA Research Associate at Lewis Research Center); Bruce A. Reichert, Kansas State University, Department of Mechanical Engineering, Manhattan, Kansas 66502; Jeffry D. Foster, Iowa State University, Mechanical Engineering Department, Ames, Iowa 50010 and NASA Resident Research Associate at Lewis Research Center. Project Manager, John M. Abbott, Internal Fluid Mechanics Division, organization code 2660, (216) 433–3607.

12a. DISTRIBUTION/AVAILABILITY STATEMENT

Unclassified - Unlimited
Subject Category 02
This publication is available from the NASA Center for Aerospace Information, (301) 621–0390.

12b. DISTRIBUTION CODE

13. ABSTRACT ***(Maximum 200 words)***

An experimental study is conducted to examine the crossplane structure and streamwise decay of vortices shed from airfoil-type vortex generators. The vortex generators are set in a counter-rotating array spanning the full circumference of a straight pipe. The span of the vortex generators above the duct surface, h, is approximately equal to the local turbulent boundary layer thickness, δ. Measurement of three-component mean flow velocity in downstream crossplanes are used to characterize the structure of the shed vortices. Measurements in adjacent crossplanes (closely spaced along the streamwise coordinate) characterize the interaction and decay of the embedded vortices. A model constructed by the superposition of Oseen vortices is compared to the data for one test case.

14. SUBJECT TERMS	15. NUMBER OF PAGES
Vortices; Vortex generators; Three dimensional boundary layer	13
	16. PRICE CODE: A03

17. SECURITY CLASSIFICATION OF REPORT	18. SECURITY CLASSIFICATION OF THIS PAGE	19. SECURITY CLASSIFICATION OF ABSTRACT	20. LIMITATION OF ABSTRACT
Unclassified	Unclassified	Unclassified	